# Optimal Electric Power Take-off Strategy for Surface Riding Wave Energy Converter


Shrikesh Sheshaprasad
*Dept. of Elec. & Comp. Eng*
*Texas A&M University*
College Station, USA
shrikesh@tamu.edu

Farid Naghavi
*Dept. of Elec. & Comp. Eng*
*Texas A&M University*
College Station, USA
faridnaghavi@tamu.edu

Shima Hasanpour
*Dept. of Elec. & Comp. Eng*
*Texas A&M University*
College Station, USA
shimahasanpour@tamu.edu

Mesaad Albader
*Dept. of Elec. & Comp. Eng*
*Texas A&M University*
College Station, USA
malbader@tamu.edu

Matthew C Gardner
*Dept. of Elec. & Comp. Engr.*
*University of Texas at Dallas*
Richardson, TX, USA
Matthew.Gardner@utdallas.edu

HeonYong Kang
*Dept. of Ocean. Eng*
*Texas A&M University*
College Station, USA
ga0prodg@tamu.edu

Hamid A Toliyat
*Dept. of Elec. & Comp. Eng*
*Texas A&M University*
College Station, USA
toliyat@tamu.edu



***Abstract*— Surface Riding Wave Energy Converters (SR-WEC) are energy conversion devices that utilize a linear generator to harness wave energy at a low Levelized Cost of Energy (LCOE). The SR-WEC has its own set of challenges in terms of power take-off (PTO). This paper discusses the optimization of various types of electric power take-off (PTO) strategies, such as passive, reactive, and binary PTO, for the SR-WEC. A novel and optimal PTO strategy called the binary-reactive PTO, is proposed for the SR-WEC. The performance of each strategy is compared using results based on a given wave elevation dataset. A Simulink model is built to validate the time domain simulations with non-idealities of the linear generator. The PTO strategies are also implemented using a testbed with a permanent magnet linear generator. From the simulation results, it is seen that the novel binary-reactive provides the most optimal PTO for the SR-WEC application.**



***Keywords—Wave energy converter, power take-off strategies, linear generator, passive PTO, reactive PTO, binary PTO, binary-reactive PTO.***


## I. Introduction

The energy demand in today's world is constantly rising. There is a need for clean, renewable sources of energy at affordable cost. One renewable source is the ocean waves. Ocean waves contain a substantial amount of energy. Waves are generated as a result of winds blowing on the ocean surface. These winds are caused by the redistribution of solar energy. Waves can build up over time and reach energy densities averaging over 100 kW/m. [1]. Some estimates show that it is technologically feasible to harvest approximately 6% of the national energy demand of the U.S from the wave energy that reaches its coastline [2]. Wave energy converters (WEC) are energy capture devices that harness the kinetic energy of the ocean waves and convert them into useful mechanical or electrical energy. WECs were conceptualized as early as 1799 [3]. According to a review in 2015, there were at least 170 WECs in various stages of development [4]. Several different types of wave energy converters have been discussed in [3] - [8]. The recently invented surface riding wave energy converter (SR-WEC) [9] provides a new approach to convert wave energy to renewable electricity in small or intermediate scales with competitive levelized cost of energy (LCOE).

This paper discusses the SR-WEC and the various power take-off (PTO) strategies. It also introduces a novel PTO strategy that is optimized for maximum energy capture from the SR-WEC. Simulation and experimental validation of the optimal PTO strategies are also provided.

## II. Surface Riding Wave Energy Converter

Fig. 1 shows the basic structure of the SR-WEC. The SR-WEC consists of an outer cylinder housing a permanent magnet (PM) linear generator [10]. The generator has a stator made of copper windings and a PM translator sliding on a center rod. The relative invariance of the wave slopes throughout different sea states allows an inherently extended operating window in annual operation, and the rotational tilting motions make resonance control easier through relocating a mass [11]. To resonate the tilt motion with varying incident wave frequencies, movable rings in the buoyancy unit can be relocated such that the natural frequency of the tilt coincides with that of the incident wave. This gives the SR-WEC an advantage over other forms of WECs since it can extract energy from a wide range of incident wave frequencies. To ensure reliable long-term production with a simple system [12], the PM linear generator is sealed inside the cylinder, which improves survivability beyond other existing wave energy converters with generation interfaces exposed to the ocean waves.

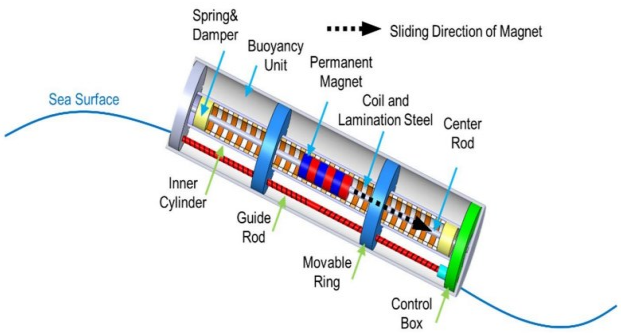


Fig. 1. Surface riding wave energy converter


Research was sponsored by the Department of Energy under Grant No. DE-EE0008630

The SR-WEC rides on the surface of the ocean waves and is pitched up and down as the wave elevation changes. As the wave elevation ($\theta_{wave}$) changes, the translator is pushed across the length of the tube. The translator experiences a force:

$$F_{excitation} = mg \sin \theta_{tube} \quad (1)$$

where $m$ is the mass of the translator, $\theta_{tube}$ is the elevation angle of the SR-WEC and $g$ is the gravitational acceleration constant. This force accelerates the PM translator, and the resulting kinetic energy is harnessed through the windings of the linear generator.

The speed of the sliding mass can be found by using:

$$speed(x+1) = speed(x) + \Delta t * (F_{excitation} + F_{PTO})/m \quad (2)$$

where, $x$ is the current time index, $\Delta t$ is the time step of computation, and $F_{PTO}$ is the PTO force. Similarly, the position of the sliding mass can be estimated using:

$$pos(x+1) = pos(x) + \Delta t \frac{[speed(x) + speed(x+1)]}{2} \quad (3)$$

Based on the values of $\theta_{tube}$, $speed$, and $pos$, the PTO force, $F_{PTO}$ is determined under the different PTO strategies.

## III. Power Take-off Strategies

The power take-off (PTO) strategy is responsible for ensuring that the WEC is utilized in the most effective manner by extracting as much electrical energy from the waves as possible. Various PTO damping strategies are discussed in [13]-[15]. These include passive, reactive and discrete PTO strategies. The intensity and duration of force applied on the translator during energy harvesting is set by the PTO strategy. Thus, these strategies play an important role in determining the average output power generation. In the SR-WEC, the linear generator is able to apply the PTO force by controlling the current through the windings. Unlike WECs that use a rotary machine for energy capture, the SR-WEC does not have cyclic motion of the PMs. The linear generator has a limited sliding distance with a fixed force and power constraints. Therefore, it is important to study the effectiveness of conventional PTO strategies.

### A. Passive PTO Control

One of the simplest forms of PTO is loading the SR-WEC passively. This replicates a simple viscous damping of the sliding motion. The force applied on the PM translator is directly proportional to its speed. The PTO force is given by:

$$F_{PTO} = -C_{PTO}\dot{X}_{rel}, \quad (4)$$

Where $F_{PTO}$ is the PTO force applied by the generator, $C_{PTO}$ is the viscous damping coefficient, and $\dot{X}_{rel}$ is the speed of the sliding mass relative to the stator. While applying the $F_{PTO}$, it is also important to ensure that the power and force limits of the system are not exceeded. The passive PTO force and the corresponding speed and position of the PM translator is shown in Fig. 2(a). It can be seen that the force is directly proportional to the speed of the PM translator. Note that the speed suddenly goes to zero when the translator hits the end of the tube.

### B. Reactive PTO Control

Reactive PTO is where the PTO force has two components. One is proportional to the relative speed of the translator, and the other is proportional to the position. This replicates a viscous damper along with a stiffness spring. The reactive PTO for force is given by:

$$F_{PTO} = -K_{PTO}X_{rel} - C_{PTO}\dot{X}_{rel} \quad (5)$$

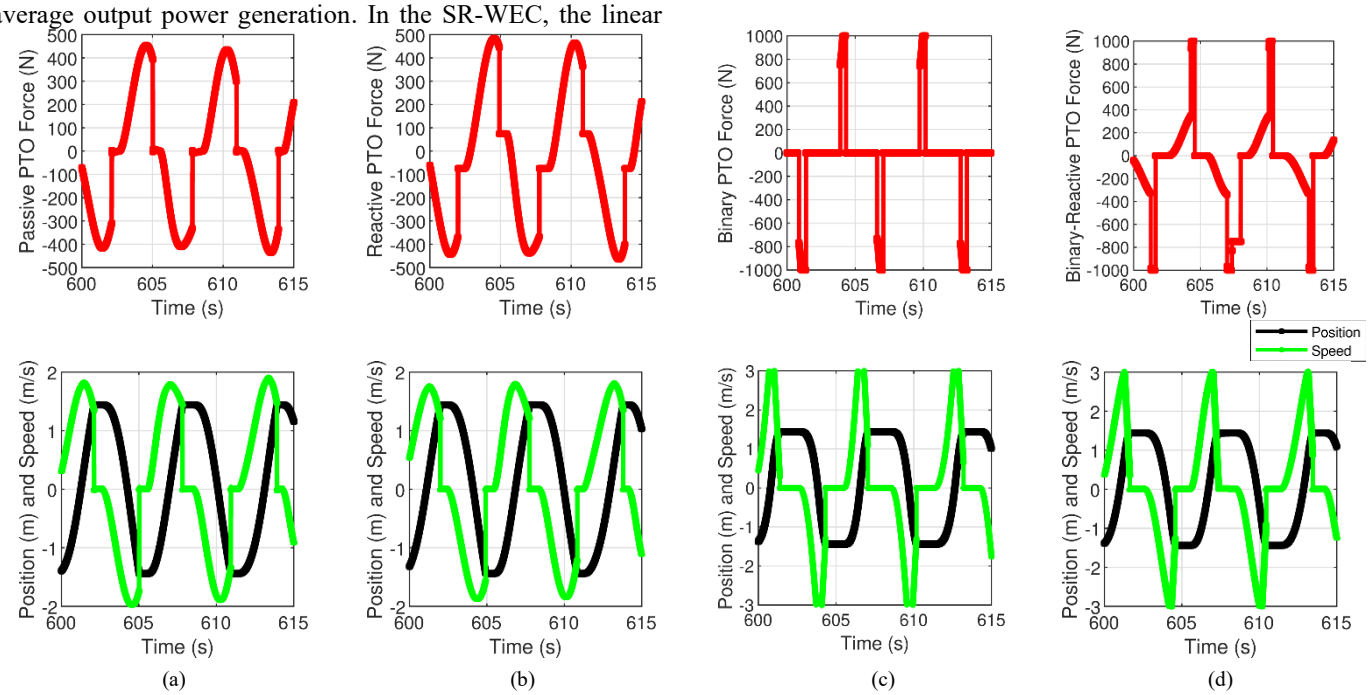


Fig. 2. Ideal time domain simulation: PTO force and corresponding position and speed of PM translator: (a) passive, (b) reactive, (c) binary, and (d) binary-reactive PTO strategies

where $K_{PTO}$ is the stiffness coefficient and $X_{rel}$ is the position of the sliding mass relative to the stator. Thus, the generator emulates both an electrical spring and an electrical viscous damper. If the impedance of the translator's mass is matched by the impedance of the PTO stiffness coefficient, maximum power capture can be achieved. As passive PTO, it is important to ensure that the force and power limits are not exceeded while applying the PTO force on the PM translator. The application of reactive PTO force and the corresponding speed and position of the PM translator is shown in Fig. 2(b). It can be seen that the force is a function of both speed and position of the translator.

In a reactive PTO implementation, a bidirectional power flow is required between the DC bus and the linear generator. In order to effectively match the impedance of the PTO to that of the wave impedance, the $K_{PTO}$ coefficient needs to be set according to (6).

$$K_{PTO} = slidingMass * \left(\frac{2\pi}{peakPeriod}\right)^2 \quad (6)$$

where, $slidingMass$ is the mass of the PM translator, and $peakPeriod$ is the peak period of the given wave. Typically, reactive PTO is seen to be the most optimal under the assumption of a purely sinusoidal incident wave [14]. However, under irregular wave conditions, and the limited sliding distance in the SR-WEC, the reactive damping fails to provide the optimal PTO output.

### C. Binary PTO Control

Binary PTO damping is a strategy where the generator is in either an ON or OFF state. Whenever the generator is ON, it generates the maximum instantaneous power, subject to its force and power ratings. This generator is turned ON whenever the sliding mass approaches the end of the tube or when the tube changes its direction of tilt such that the mass is sliding uphill. The generator is then turned off when the sliding mass is brought to a stop. A binary timing term called the *binary factor* is used to control how early or late the generator is turned ON before hitting the ends of the tube. The force profile of the binary PTO along with the position and speed values of the PM translator is shown in Fig. 2(c). It can be seen that as the translator reaches the ends of the tube, the generator is turned ON to apply maximum force. The flowchart in Fig. 3 shows the conditions under which the binary PTO is turned ON.

### D. Binary-Reactive PTO Control

Binary-reactive PTO is a combination of the binary damping and the reactive damping discussed earlier. This strategy applies a continuously varying reactive PTO force based on the position and speed of the sliding mass and when the binary damping conditions are met, the maximum power is extracted from the PM translator. Fig. 2(d) shows the force profile of a binary-reactive PTO application and the corresponding position and speed values. It can be seen that the algorithm applies a force proportional to the position and speed while the translator is near the center of the tube and applies the maximum force as the mass is about to hit the ends of the tube.

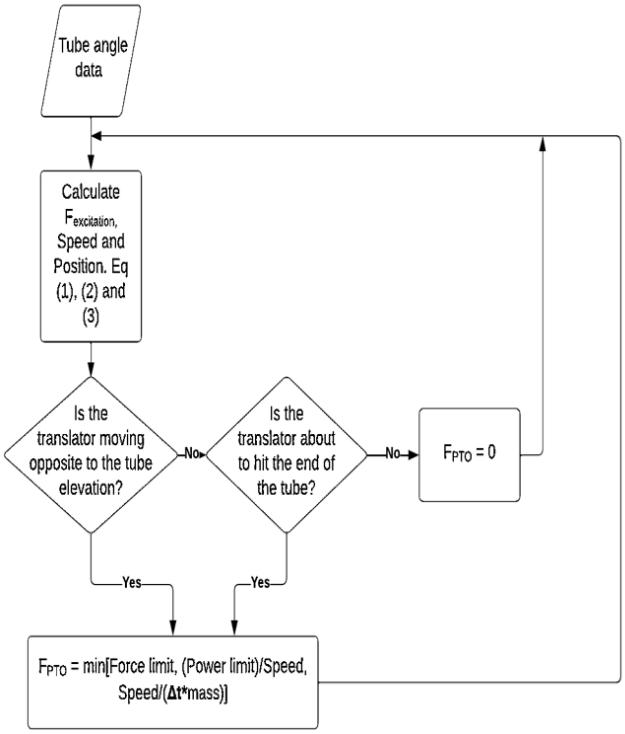


Fig. 3. Flowchart for binary PTO algorithm

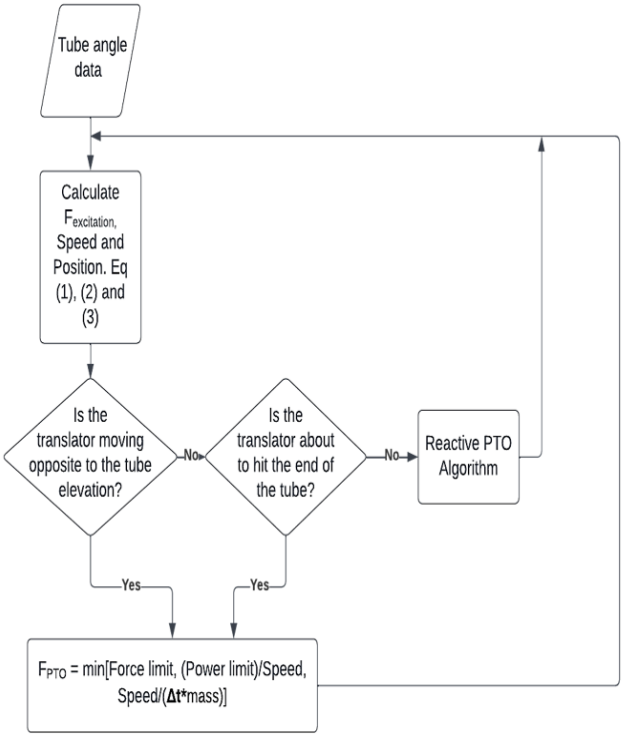


Fig.4. Flowchart for binary-reactive PTO algorithm

The flowchart in Fig. 4 shows how the PTO force is determined using binary-reactive PTO algorithm.

## IV. PTO Optimization

In order to compare the different PTO strategies, a wave data set was collected from National Data Buoy Center (NDBC) buoy #41002, located off the coast of Wilmington, North Carolina [16]. The resource characteristic bin of the wave data is shown in Table I [10]. This table provides the percentage of total data points that occurs in the given bin of significant wave height and energy period. From this dataset, 11 random sea states with varying peak periods (4.06 s to 15.7 s with an interval of 1.16 s) were used. These 11 peak periods constitute 99.79% of all data points from this buoy, representing a broad range of waves for use. Using coupled time domain simulation of the SR-WEC, the time series of tilting motion is obtained. Fig. 5 shows the resulting tube slopes for a period of time. The PM linear generator is rated for 3 kW, 1000 N of continuous operation. The selection of the PM linear generator's ratings is shown in [10]. Based on a 1200 s long time series dataset of the tilting motion, the parameters for the four PTO control algorithms were optimized to maximize average output power.

The PTO optimization involves tuning the damping coefficients for the passive, reactive, and binary reactive PTOs, and selecting the optimal *binary factor* for the binary and binary-reactive PTOs. The viscous damping and stiffness coefficients are determined by running an extensive parametric sweep of the PTO coefficients for each time period and choosing the values that provided the maximum average output power for the majority of the wave spectrum. A ballpark starting point for $K_{PTO}$ is chosen using the impedance matching equation (6) and then sweeping the variable around this point. While optimizing the reactive PTO algorithm for random waves, the $peakPeriod$ is set by performing a spectrum analysis of the waves and determining the dominant period in the time series. The $C_{PTO}$ coefficient is parametrically varied within a set range.

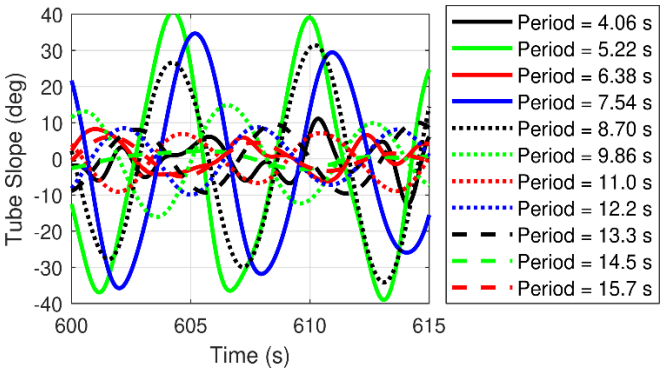


Fig. 5. Tube slope data

As mentioned in Section III, the binary PTO is optimized by including a binary timing term called the *binary factor* that determines how early or late the PTO force is turned ON as the translator approaches the end of the tube. This number is a fraction of the tube length, and it is parametrically varied to find the best value providing the maximum average output power. Binary-reactive PTO optimization involves a combination of both reactive and binary parts of the system.

### A. Comparison

The four PTO strategies were optimized for the given dataset. Since the dataset is representative of the real-world conditions that will be encountered by the SR-WEC in the sea, it can be used to represent the power generation capability of the SR-WEC at that location for the lifetime of its operation. These

TABLE I RESOURCE CHARACTERISTIC BIN OF THE WAVE DATA [10]

| | | Energy Period $T_e$(s) | | | | | | | | | | |
|---|---|---|---|---|---|---|---|---|---|---|---|---|
| | Occurrence % | 3.5 | 4.5 | 5.5 | 6.5 | 7.5 | 8.5 | 9.5 | 10.5 | 11.5 | 12.5 | 13.5 |
| Significant Wave Height $H_s$ (m) | 0.25 | 0.00 | 0.00 | 0.07 | 0.18 | 0.23 | 0.00 | 0.00 | 0.00 | 0.00 | 0.00 | 0.00 |
| | 0.75 | 0.44 | 2.42 | 2.38 | 4.85 | 7.47 | 0.89 | 0.63 | 0.36 | 0.32 | 0.00 | 0.00 |
| | 1.25 | 0.61 | 5.57 | 8.11 | 3.88 | 8.84 | 1.28 | 1.10 | 0.30 | 0.36 | 0.00 | 0.01 |
| | 1.75 | 0.01 | 1.18 | 5.36 | 4.44 | 5.35 | 1.43 | 1.14 | 0.33 | 0.30 | 0.00 | 0.11 |
| | 2.25 | 0.00 | 0.15 | 2.13 | 3.69 | 2.43 | 0.39 | 0.67 | 0.15 | 0.23 | 0.10 | 0.01 |
| | 2.75 | 0.00 | 0.00 | 0.74 | 2.21 | 2.97 | 0.41 | 0.54 | 0.18 | 0.21 | 0.07 | 0.04 |
| | 3.25 | 0.00 | 0.00 | 0.10 | 1.27 | 2.43 | 0.44 | 0.23 | 0.11 | 0.06 | 0.12 | 0.06 |
| | 3.75 | 0.00 | 0.00 | 0.01 | 0.33 | 1.27 | 0.28 | 0.17 | 0.06 | 0.15 | 0.14 | 0.12 |
| | 4.25 | 0.00 | 0.00 | 0.00 | 0.04 | 0.61 | 0.36 | 0.25 | 0.03 | 0.10 | 0.11 | 0.12 |
| | 4.75 | 0.00 | 0.00 | 0.00 | 0.00 | 0.33 | 0.25 | 0.26 | 0.00 | 0.03 | 0.14 | 0.15 |
| | 5.25 | 0.00 | 0.00 | 0.00 | 0.00 | 0.06 | 0.12 | 0.17 | 0.03 | 0.06 | 0.12 | 0.12 |
| | 5.75 | 0.00 | 0.00 | 0.00 | 0.00 | 0.10 | 0.11 | 0.12 | 0.04 | 0.08 | 0.07 | 0.03 |
| | 6.25 | 0.00 | 0.00 | 0.00 | 0.00 | 0.03 | 0.04 | 0.11 | 0.04 | 0.03 | 0.06 | 0.21 |
| | 6.75 | 0.00 | 0.00 | 0.00 | 0.00 | 0.00 | 0.03 | 0.03 | 0.06 | 0.07 | 0.07 | 0.14 |
| | 7.25 | 0.00 | 0.00 | 0.00 | 0.00 | 0.00 | 0.00 | 0.01 | 0.00 | 0.08 | 0.03 | 0.08 |
| | 7.75 | 0.00 | 0.00 | 0.00 | 0.00 | 0.00 | 0.00 | 0.00 | 0.00 | 0.01 | 0.03 | 0.00 |
| | 8.25 | 0.00 | 0.00 | 0.00 | 0.00 | 0.00 | 0.00 | 0.00 | 0.00 | 0.01 | 0.00 | 0.01 |
| | 8.75 | 0.00 | 0.00 | 0.00 | 0.00 | 0.00 | 0.00 | 0.00 | 0.00 | 0.00 | 0.01 | 0.00 |
| | 9.25 | 0.00 | 0.00 | 0.00 | 0.00 | 0.00 | 0.00 | 0.00 | 0.00 | 0.00 | 0.00 | 0.00 |
| | 9.75 | 0.00 | 0.00 | 0.00 | 0.00 | 0.00 | 0.00 | 0.00 | 0.00 | 0.00 | 0.00 | 0.00 |
| Peak Period $T_p$(s) | | 4.06 | 5.22 | 6.38 | 7.54 | 8.7 | 9.86 | 11.02 | 12.18 | 13.34 | 14.5 | 15.66 |

TABLE II - AVERAGE POWER OUTPUT FOR DIFFERENT PTO STRATEGIES

| | Average output power (W) | | | |
|---|---|---|---|---|
| **Peak period (s)** | **Passive PTO** | **Reactive PTO** | **Binary PTO** | **Binary-Reactive PTO** |
| **4.06** | 17.67 | 36.25 | 42.38 | 85.22 |
| **5.22** | 330.47 | 334.79 | 355.75 | 364.68 |
| **6.38** | 86.59 | 100.33 | 134.82 | 128.28 |
| **7.54** | 131.30 | 141.39 | 185.31 | 167.85 |
| **8.70** | 204.56 | 212.51 | 261.15 | 244.39 |
| **9.86** | 62.33 | 79.44 | 104.86 | 107.94 |
| **11.0** | 100.44 | 116.33 | 152.78 | 147.57 |
| **12.2** | 30.21 | 46.94 | 58.80 | 67.66 |
| **13.3** | 37.56 | 55.80 | 70.11 | 78.75 |
| **14.5** | 19.91 | 39.07 | 44.14 | 58.62 |
| **15.7** | 13.26 | 28.10 | 29.37 | 44.59 |
| **Weighted Average** | 70.74 | 84.81 | 103.69 | 108.39 |

numbers do not account for the efficiencies of the linear generator or the controlled rectifier, as that is a variable controlled by the optimal design of the machine and power electronics. Additionally, these analyses assume that the generator is able to follow the force command instantaneously or, equivalently, that the DC bus voltage used is very large, allowing rapid changes in the current. The averaging for the power is done only on the second half of the dataset as the first half includes the ramping up of the hydrodynamic simulation, which is a transient state. The average power outputs of each sea state for each PTO strategy is tabulated in Table II.

It is seen that passive PTO produces the least average power across all sea states. This is in line with the literature that passive damping is sub-optimal for energy capture from both regular and random waves. Reactive PTO produces significantly better average power output for a majority of the sea states and smaller gains are seen in other sea states. This bolsters the argument that output power is improved when using reactive PTO over passive PTO strategy. Given the nature of the SR-WEC with a limited sliding distance and under random wave excitation, the reactive PTO is not the most optimal. A more discrete strategy is better suited. This can be seen by the increase in output power for the binary PTO. There is a significant improvement in average output power in the binary PTO compared to reactive PTO. When a combination of reactive and binary algorithms is used in the form of binary-reactive PTO, the power output is seen to be better in the majority of sea states. The weighted average is calculated by multiplying the average power in each state with its corresponding percentage of occurrence taken from Table I. The average output of binary-reactive PTO is about 4.5% improvement over the binary PTO.

## V. SIMULINK AND HARDWARE VERIFICATION

### *A. Simulink Model*

A Simulink model was built to verify the controllability of a PM linear machine. The PM machine was modelled with non-idealities, which include winding resistance and winding inductance. The field oriented control (FOC) scheme was used to control the force on the PM translator. The wave slope data from NDBC was used to simulate the wave input, and the four PTO strategies were applied. The controller was able to track and apply the commanded forces on the PM translator as dictated by the PTO strategies. The applied forces, and corresponding speed and position are shown in Fig 6.

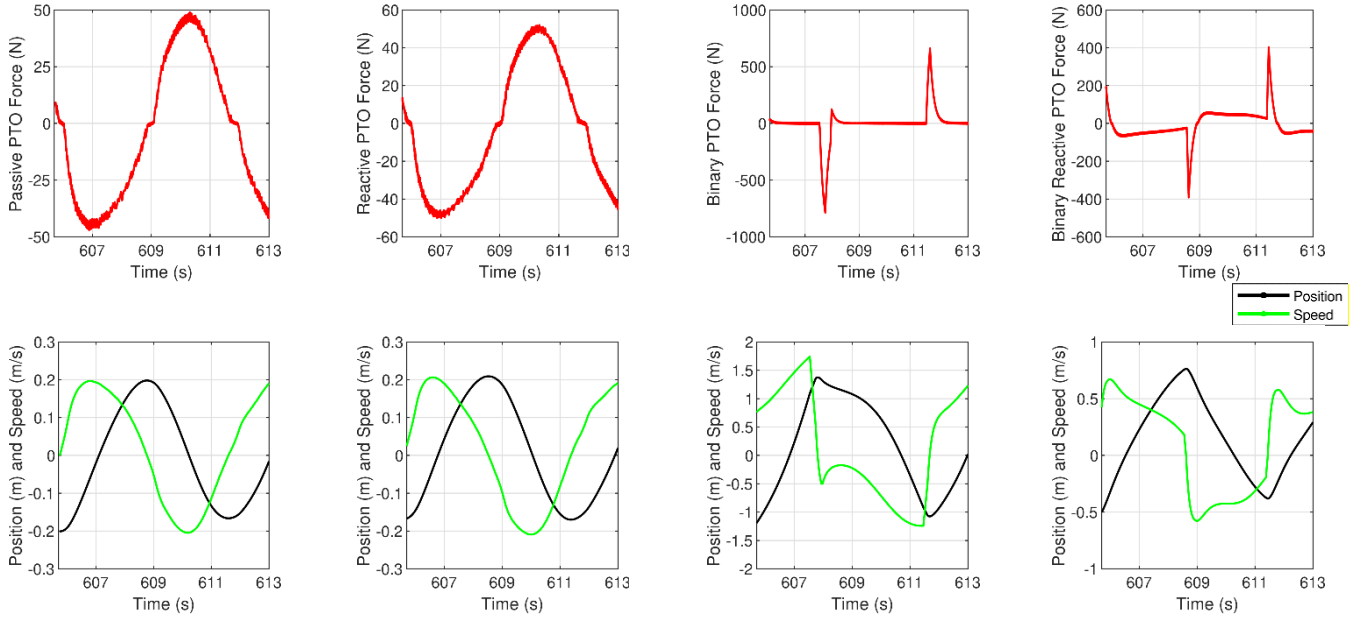


Fig. 6. Simulink output: PTO force and corresponding position and speed of PM translator for (a) passive, (b) reactive, (c) binary, and (d) binary-reactive PTO strategies

### B. Hardware Setup

The implementation of PTO algorithm was verified on a testbed shown in Fig. 7. This setup consists of a PM linear machine that was used as a generator, a rotary machine acting as a prime mover, and a Trans-rotary Magnetic Gear (TROMAG) [17] that was used to couple the rotary and the linear machines. The linear machine consists of a long surface permanent magnet (SPM) translator and a shorter copper wound stator. A sensorless (FOC) algorithm was used to control the linear generator [18]. This system is a scaled down version of the full scaled model considered for the results in section IV. The PTO was scaled according to the scaling laws described in [19].

Fig. 7. Testbed setup

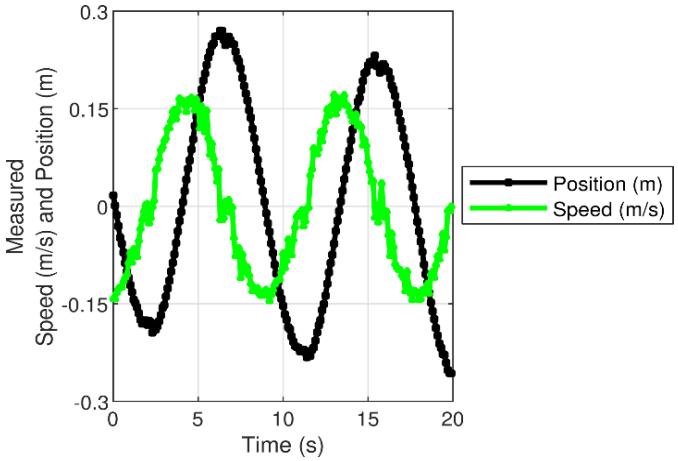

Fig. 8. Measured speed and position of the PM translator.

The rotary machine controlled the excitation forces. For the test, a sinusoidal excitation was commanded. It should be noted that the machine's speed was controlled using a closed loop FOC. Therefore, the speed does not change with the application of PTO force, like it would in the SR-WEC. The position and speed of the PM translator are measured using a linear encoder and are shown in Fig. 8. For an SPM machine, the force on the translator is directly proportional to the q-axis current in the stator. Therefore, the PTO force is commanded by the corresponding q-axis current in the linear generator.

The four PTO strategies were applied to the testbed under the given excitation. The measured q-axis current for the passive, reactive, binary, and binary-reactive PTO is shown in Fig. 9. This shows the feasibility of applying the various PTO forces on a PM linear generator using the vector control.

## VI. Conclusion

In this paper, the functioning of the SR-WEC was discussed. The conventional PTO algorithms and their application for the SR-WEC were presented. The novel binary-reactive PTO was introduced. The time domain simulations of four different PTO was carried out based on NDBC datasets and the simulation results show that the binary-reactive PTO is the most optimal for the SR-WEC given the limited tube length and the nonsinusoidal waves. A Simulink model was built to test the controllability of the PM linear generator. The hardware setup was used to show the implementation of PTO algorithm on a linear machine. The application of PTO force according to the different algorithms was demonstrated.

## Acknowledgment

This material was based on the work supported by Department of Energy under Award Number DE- EE0008630. This report was prepared as an account work sponsored by an agency in United States Government. Neither the United States Government nor any agency thereof, nor any their employees, makes any warranty, express or implied, or assumes any legal liability or responsibility for the accuracy, completeness, or usefulness of any information, apparatus, product, or process disclosed, or represents its use would not infringe privately owned rights. Reference herein to any specific commercial product, process, or service by trade name, trademark, manufacturer, or otherwise does not necessarily constitute or imply its endorsement, recommendation, or favoring by the United States Government or any agency thereof. The views and opinions of authors expressed herein do not necessarily state or reflect those of the United States Government or any agency thereof.

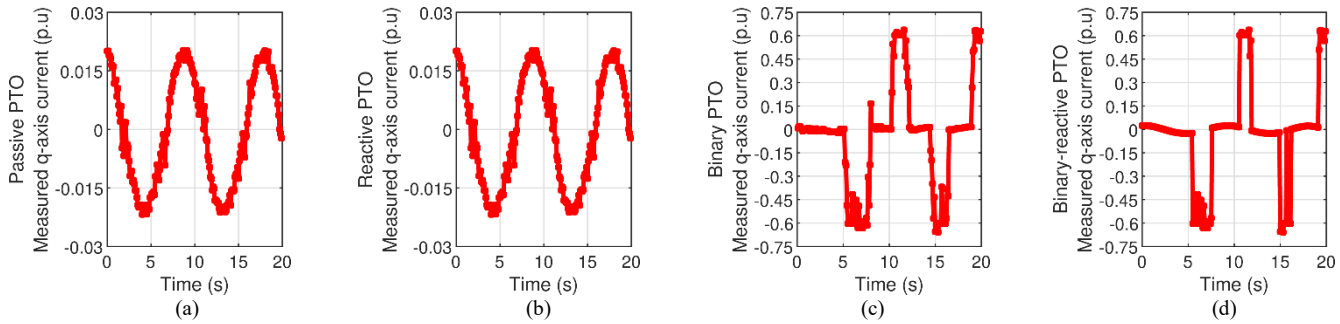

Fig. 9. Measured per unit q-axis Current for (a) Passive, (b) Reactive, (c) Binary, and (d) Binary-Reactive PTO Strategies

## REFERENCES


[1] S. Barstow, G. Mørk, D. Mollison, and J. Cruz, "The Wave Energy Resource," in *Ocean Wave Energy: Current Status and Future Prespectives*, J. Cruz Ed. Berlin, Heidelberg: Springer Berlin Heidelberg, 2008, pp. 93-132.

[2] R. Bedard *et al.*, "North American ocean energy status-March 2007," *Electric Power Research Institute (EPRI) Tidal Power (TP),* vol. 8, p. 17, 2007.

[3] A. Clément *et al.*, "Wave energy in Europe: current status and perspectives," *Renewable and sust. energy rev.,* vol. 6, no. 5, pp. 405-431, 2002.

[4] D. Magagna and A. Uihlein, "Ocean energy development in Europe: Current status and future perspectives," *Int. J. of Marine Energy,* vol. 11, pp. 84-104, 2015.

[5] J. Falnes, "A review of wave-energy extraction," *Marine structures,* vol. 20, no. 4, pp. 185-201, 2007.

[6] S. Prakash *et al.*, "Wave energy converter: a review of wave energy conversion technology," in *Proc. Asia-Pacific World Congr. on Comput. Sci. and Eng.*, 2016, pp. 71-77.

[7] T.W. Thorpe, "An overview of Wave Energy Technologies: Status, Performance and Costs," *Wave Power – Moving Towards Commercial Viability* – IMECHE Seminar, London, US, 1999.

[8] H. Titah-Benbouzid and M. Benbouzid, "Ocean wave energy extraction: Up-to-date technologies review and evaluation," in *Proc. Int Power Electron. and Appl. Conf. and Expo.*, 2014, pp. 338-342.

[9] H. Kang and M. Kim, "Method and apparatus for wave energy conversion," US Patent 10,352,290, 2019.

[10] F. Naghavi, S. Sheshaprasad, M. Gardner, A. Meduri, H. Kang, and H. Toliyat, "Permanent Magnet Linear Generator Design for Surface Riding Wave Energy Converters," in *Proc. IEEE Energy Convers. Congr. and Expo.*, 2021, pp. 4369-4375.

[11] C. Jin, H. Kang, M. Kim, and F. P. Bakti, "Performance evaluation of surface riding wave energy converter with linear electric generator," *Ocean Eng.*, vol. 218, pp. 108141, Dec. 2020.

[12] N. Hodgins, O. Keysan, A. S. McDonald, and M. A. Mueller, "Design and testing of a linear generator for wave-energy applications," *IEEE Trans. on Ind Electron.,* vol. 59, no. 5, pp. 2094-2103, 2011.

[13] E. Anderlini, D. I. M. Forehand, P. Stansell, Q. Xiao and M. Abusara, "Control of a Point Absorber Using Reinforcement Learning," *IEEE Trans. on Sust. Energy*, vol. 7, no. 4, pp. 1681-1690, Oct. 2016.

[14] P. Kracht, S. Perez-Becker, J. Richard and B. Fischer, "Performance Improvement of a Point Absorber Wave Energy Converter by Application of an Observer-Based Control: Results From Wave Tank Testing," in *IEEE Trans. on Ind. App.*, vol. 51, no. 4, pp. 3426-3434, Aug. 2015.

[15] E. Tedeschi and M. Molinas, "Tunable Control Strategy for Wave Energy Converters With Limited Power Takeoff Rating," in *IEEE Trans. on Ind. Electron*., vol. 59, no. 10, pp. 3838-3846, Dec. 2011.

[16] National Oceanic and Atmospheric Administration. [Online]. Available: https://www.ndbc.noaa.gov/station_history.php?station=41002

[17] S. Pakdelian, N. W. Frank, and H. A. Toliyat, "Principles of the trans-rotary magnetic gear," *IEEE Trans. on Magn.,* vol. 49, no. 2, pp. 883-889, 2012.

[18] H. A. Hussain and H. A. Toliyat, "Back-EMF based sensorless vector control of tubular PM linear motors," in *2015 IEEE Int. Elect. Mach. & Drives Conf.*, 2015, pp. 878-883.

[19] G. Giannini, *et al*, "Wave Energy Converter Power Take-Off System Scaling and Physical Modelling" *J. of Marine Sci. and Eng.*, vol. 8, no. 9, p 632, 2020.